第 48 卷 第 10 期
2021 年 10 月

湖南大学学报（自然科学版）
Journal of Hunan University (Natural Sciences）

Vol. 48 No. 10
October 2021

Open Access Article

Effect of Reinforcement Type, Diaphragms, and Hollow Core on the Torsional Capacity of HSC Box-Girders under Torsion, Shear, and Bending

Mariwan Mirhaj Mohamed-Salih[1*], Ali Ramadhan Yousif[2]

[1] Ph.D. student, Department of Civil Engineering, Salahaddin University-Erbil, Erbil, Iraq

[2] Department of Civil Engineering, Salahaddin University-Erbil, Iraq

Abstract: To date, no research has been conducted on high-strength concrete (HSC) box-girders reinforced with basalt fiber reinforced polymer (BFRP) rebars and steel stirrups under combined actions of torsion, shear, and bending. In this work, rectangular HSC box-girders utilized with BFRP bars as internal longitudinal reinforcement under the combined state of loading are studied exclusively. A steel-reinforced (control) specimen and three other rectangular HSC box-girders made of BFRP bars and steel stirrups were tested under combined torsion, shear, and bending loading. Every specimen was 500 mm wide by 375 mm high, with a constant wall thickness of 120 mm, a total length of 5000 mm. Each contained about 2.5 percent total reinforcement, equally distributed between the longitudinal bars and transverse steel stirrups. The study aims to evaluate the torsional behavior of HSC box-girders considering the effect of longitudinal reinforcement type, provision or elimination of diaphragms, and the method of filling the hollow core. The experimental findings show that replacement of longitudinal steel bars with BFRP bars result in a drop in the ultimate torsional capacity by 15 percent; in addition, while the deflections at comparable loadings were lower in the entirely steel-reinforced specimen, but surprisingly, the final deflections were less in the BFRP-replaced case. When the diaphragms are eliminated, the ultimate capacities drop significantly by about half of that of a comparable specimen with diaphragms. When the hollow cores were left unfilled with Styrofoam, the ultimate capacity decreased by 30 percent with comparable twist angles but lower deflections at failure.

Keywords: box-girder, high-strength concrete, fiber-reinforced polymer bar, torsion, combined loading.

钢筋类型、隔膜和空心芯对 HSC 箱梁在扭转、剪切和弯曲作用下的抗扭能力的影响

摘要：迄今为止，迄今为止，尚未对玄武岩纤维增强聚合物（BFRP）钢筋和钢箍筋在扭转、剪切和弯曲的联合作用下增强的高强度混凝土（HSC）箱形梁进行研究。在目前的工作中，HSC 箱梁与 BFRP 钢筋用作组合荷载状态下的内部纵向钢筋。在扭转、剪切和弯曲的联合载荷下测试了一个钢筋（对照）试样和其他三个由 BFRP 钢筋和钢箍制成的矩形 HSC 箱形梁。每个试样宽 500 毫米，高 375 毫米，壁厚恒定为 120 毫米，总长度为 5000 毫米，每个试样包含约 2.5% 的总钢筋，平均分布在纵向钢筋和横向钢箍筋之间。该研究评估了 HSC 箱梁在纵向钢筋类型、设置或消除隔板以及空心填充方法的影响下的扭转行为。试验结果表明，用 BFRP 筋代替纵向钢筋导致极限抗扭能力下降 15%；此外，虽然在可比载荷下的挠度在完全钢增强的试样中较低，但令人惊讶的是，在替换 BFRP 的情况下，最终挠度较小。当去除隔膜时，最终容量显着下降，约为具有隔膜的可比样品的一半。当空心芯没有用泡沫聚苯乙烯填充时，最终容量下降了 30%，具有可比的扭曲角，但在破坏时挠度较低。

关键词：箱梁、高强度混凝土、纤维增强聚合物棒、扭转、组合荷载.

Received: June 6, 2021 / Revised: August 8, 2021 / Accepted: September 2, 2021 / Published: October 30, 2021

About the authors: Mariwan Mirhaj Mohamed-Salih, Department of Civil Engineering, Faculty of Engineering, Koya University, Koya, Iraq; Ali Ramadhan Yousif, Department of Civil Engineering, Salahaddin University-Erbil, Iraq

Corresponding author Mariwan Mirhaj Mohamed-Salih, mariwan.mirhaj@koyauniversity.org

1. Introduction

Nowadays, fiber-reinforced polymer (FRP) bars have been introduced as a modern, state-of-the-art material used in reinforced concrete structures. FRPs are reputable for their non-corrosive, light-weight, and high-tensile strength properties, and compared to steel reinforcement, FRPs offer better solutions for the problems of steel corrosion, allow for easier transportation, handling, and application, and it could be as suitable as steel for structural reinforcement [1]. However, FRPs are non-isotropic and, hence, strong only in the main longitudinal direction, which is in the direction of the reinforcing fibers. The weakness in the transverse direction affects shear strength, dowel action of FRP bars, and bond performance when used with concrete. Besides, FRPs have no plastic behavior and yield point and behave only in a linearly elastic manner up to failure. Therefore, their failure is not ductile. From this, it can be expected that if FRP fails, there will be extensive cracking together with abrupt and catastrophic failure [2]. As argued in [3], in contrast to steel reinforced members, for the FRP-reinforced members, there should be explicit provision to control failure by concrete crushing rather than FRP rupture. The same strategy is followed by other Codes of Practice [1, 4].

The NCHRP Report 620 [5] states that diaphragm components in box-girders aid in preventing the cross-sections from excessive distortions. Diaphragms also help in distributing wheel loads and facilitate the distribution of transverse loads. Concrete box-girders are generally provided with end diaphragms and intermediate ones. While the end diaphragms have proven to be a very successful economic detail, the intermediate diaphragms are also very useful, especially when a concentrated load is applied on a box girder over the diaphragm per se. [5] From this background, it can be deduced that the ignorance of the diaphragms might harm the strength and performance capabilities of any box girder.

Even that torsion occurs widely when any loading deviates from the shear center of the section [6], the literature which addresses the use of FRP-reinforced members under the effect of torsion includes only a limited number of experimental researches that are carried out on solid- rectangular or spandrel FRP-reinforced beams under either pure torsion or torsion with flexure only [7-15]. Accordingly, it can be said that there is no experimental research concerned with BFRP reinforced hollow members under the combined actions of torsion, shear, and flexure. Moreover, except for the Canadian standards [4], other design codes do not provide any provision for the torsional design of FRP-reinforced members. This means that very scarce, if any, experimental databases and design guidelines exist on the behavior of FRP-reinforced hollow members under combined loadings of torsion, shear, and bending, which urges for new experimentally gap-filling researches to be conducted. To date, no research has dealt with the performance of high-strength concrete box-girders reinforced with basalt fiber reinforced polymer composite (BFRP) bars and steel stirrups as internal reinforcement under the combined loadings torsion, shear, and moment. Therefore, this study mainly aims at examining the effects of reinforcement type, diaphragms, and hollow-core type on the torsional strength and stiffness, cracking pattern, and failure modes experimentally; valuable information is obtained regarding the performance of such specimens.

2. Experimental Program

2.1. Specimen Details

For the purposes of this study, four specimens out of 25 box-girder specimens from a wide-scope Ph.D. program are chosen by the authors. The cross-sections were 500 mm wide by 375 mm deep with 120 mm wall thickness and a gross length of 5000 mm for each. In general, all the specimens were reinforced with a total reinforcement ratio of 2.5 percent, equally divided longitudinally and transversally. The box-girders are denoted as B-20 (control), B-23, B-24, and B-25. B-24 had no diaphragm, meaning that it was hollow throughout. The rest were provided with two hollow parts separated by a 400 mm wide solid diaphragm in the center and another two 450 mm wide solid diaphragms at both ends. Heavier reinforcement was utilized at the diaphragms to avoid excessive cross-sectional distortions and to minimize warpage. The hollow parts are selected as test zones 1850 mm long divided symmetrically from each side of the middle span of the beam. These hollow cores were formed using low-elastic polystyrene blocks in all the specimens, excluding B-25, in which a 0.2 mm thick steel plate is formed to enclose the hollow space without any Styrofoam (polystyrene). Table 1 presents the details of the reinforcement used in each specimen. Further, the details of specimen cross-sections, their geometry, reinforcement layout, and the instrumentations used per cross-section are as shown in Figure 1.

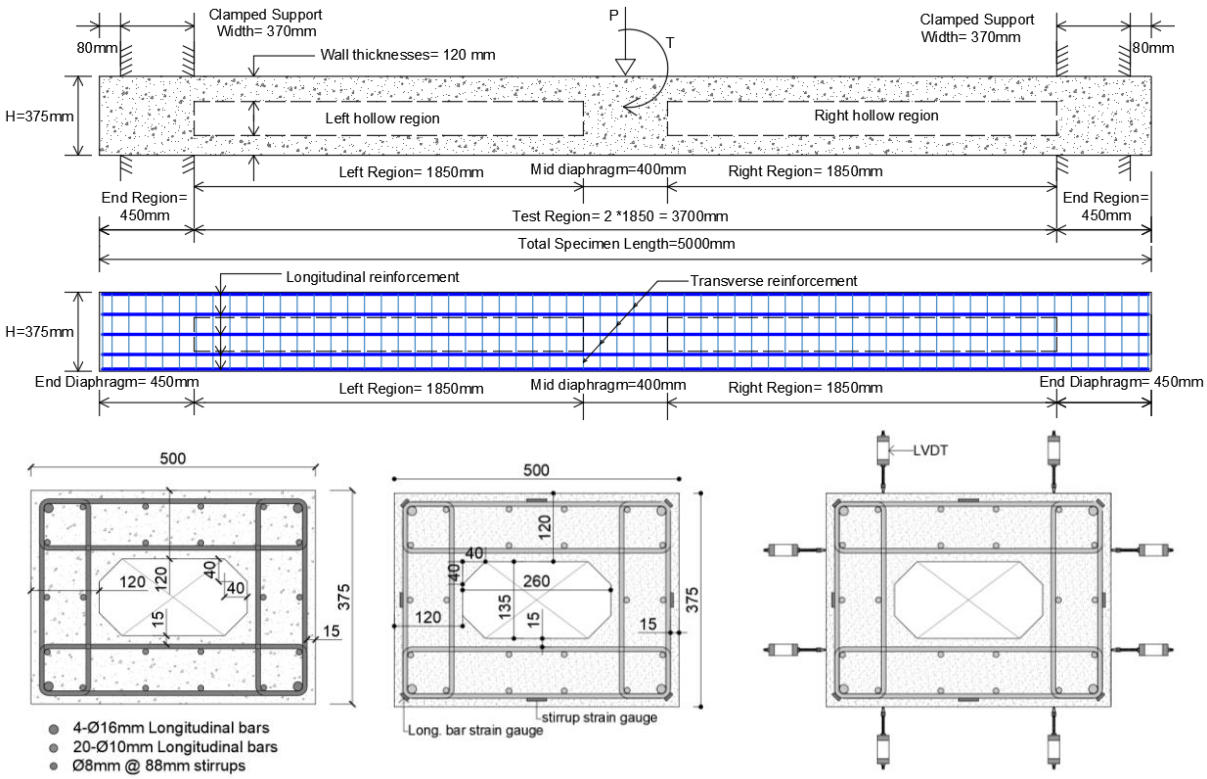

Fig. 1 Specimen details. Top-2: Longitudinal profile, Bottom-3: Reinforcement configuration & instrumentation

Table 1 Properties of box-girder specimens

#	Variables	Reinforcement		S, mm	A_l, mm^2	A_t, mm^2	$\rho_l = \frac{A_l}{A_{oh}}$,%	$\rho_t = \frac{A_t \times p_h}{s \times A_{oh}}$,%
		BFRP Bars	Stirrups					
B-20	Steel reinforcement & Styrofoam & Diaphragm	4Ø16 + 20Ø10	Ø08	88	2384	50	1.27	1.21
B-23	BFRP bars & steel stirrups & Styrofoam & Diaphragm	4Ø16 + 20Ø10	Ø08	88	2384	50	1.27	1.21
B-24	BFRP bars & steel stirrups & Styrofoam but Without	4Ø16 + 20Ø10	Ø08	88	2384	50	1.27	1.21
B-25	Diaphragm BFRP bars & steel stirrups & Diaphragm but Without Styrofoam	4Ø16 + 20Ø10	Ø08	88	2384	50	1.27	1.21

Fig. 2 Reinforcement cages

After assembling the reinforcement cages as shown in Figure 2, a total of 16 strain gauges were mounted on the longitudinal bars and steel stirrups at two sections: one at 50mm from the face of the midspan diaphragm and the other at 50mm from the face of one of the support diaphragms. Next, plywood molds were prepared, and then the reinforcement cages were positioned inside the molds and adjusted to get the required covers, and also for each hollow part, the collapsible void formers were put through to create the required hollow core. Ready-mix concrete was then used to cast the specimens together with quality-control samples (cylinders, cubes, and prisms), and all the samples were allowed 24 hours to harden, and thereafter the forms were removed. The samples, then, were kept moisturized for at least 28 days according to

the ASTM standard [16]. The box-girder specimens were then painted using acrylic emulsion paint. One of the test zones was highlighted with equal grids to facilitate detecting and recording the propagation of cracks during each test.

2.2. Material Properties

2.2.1. Concrete

The experimental program consists of using high-strength concrete (HSC) for all the specimens. Hence, the HSC concrete used to cast the specimens has been designed for a targeted 28-day cylinder compressive strength of 60 MPa. Table 2 shows the proportions used in the mix design with the maximum size of coarse aggregate of 10 mm.

Table 2 HSC mix proportions

Constituents	**Mix proportions, kg/m^3**
	Target strength, 60 MPa
Cement	550
Sand	670
Gravel	980
Water	180
Superplasticizer, Hyperplast 200	5.5

To determine the compressive strength, elastic modulus, tensile strength, and flexural strength of concrete, a range of specimens from the same batches as the main box girders were prepared and tested. Samples consisting of a total of twelve cylinders (Ø100×200) mm, six (Ø150×300) mm cylinders, six (Ø 150 × 300) mm cylinders, and a set of six (100×100×500) mm concrete prisms were prepared and tested at the Salahaddin University Laboratory at the age of 68-days to determine the required compressive strength, modulus of elasticity, tensile strength, and flexural strength of concrete, respectively. The results are as shown in Table 3. The table also shows the average values of the tested strengths at the age of 68-days, considering time-effects, the strength values at 28-days age were re-calculated using the provisions of the fib Code [17] and entered in the last column of the table for evaluation purposes.

Table 3 Properties of HSC concrete

Parameter	**Test age (day)**		**Test Standard**
	28	**68**	
Compressive strength, $f_c^{'}$, MPa	61	65.6	[18]
Density, kg/m3	2426	2426	[19]
Elastic modulus, GPa	38	39.5	[20]
Tensile strength, f_t, MPa	3	3.21	[21]
Flexural strength, f_b, MPa	6	6.59	[22]

2.2.2. BFRP Bars and Steel Stirrups

All the BFRP bars and factory-made BFRP stirrups were ordered from Chongqing Yangkai Co., China. Their technical datasheet has been provided by the same manufacturer in which all BFRP test results conform to the Chinese Standard GBT228 [23]. The conventional steel bars used to make the stirrups were ordered from a local market and tested per the ASTM standard [24]. Table 4 presents the required properties of the BFRP bars and steel stirrups. It should be noted that different codes use different limits on the yield strength of steel reinforcement to avoid brittle failure due to web concrete crushing before yielding reinforcement. The EC2 [25] limits the yield strength of torsional reinforcement to 600 MPa, whereas the ACI Code [26] limits it to a lower limit of 420 MPa.

Table 4 Properties of steel and BFRP bars

Bar dia., mm	**Type**	**f_y, MPa**	**ε_y, mm/mm**	**f_u, MPa**	**ε_y, mm/mm**	**Weight, g/m**	**Density, g/cm^3**	**E, GPa**
8	Steel	600	0.0030	954	0.222	387	7.85	200
10	Steel	446	0.0022	657	0.195	617	7.85	200
16	Steel	353	0.0017	558	0.135	1580	7.85	200
10	BFRP	-	-	1088	0.019	150	2.10	58
16	BFRP	-	-	1004	0.017	388	2.10	58

2.3. Torsion, Shear and Moment Diagrams

From a structural point of view, the applied eccentric load in this test setup will induce a simultaneous bending, shear, and torsional action. Considering the case of a fixed-fixed beam loaded by a point load and a concentrated torque at midspan, the corresponding shear, torsion, and bending diagrams are as shown in Figure 3. The analysis produces a (T:M: V) ratio of (1.67:1.11: 1), which is equivalent to an M:T ratio of (1.5:1). Depending on this ratio, it is predicted that mostly torsion-dominated cracking and failure modes will govern in each test.

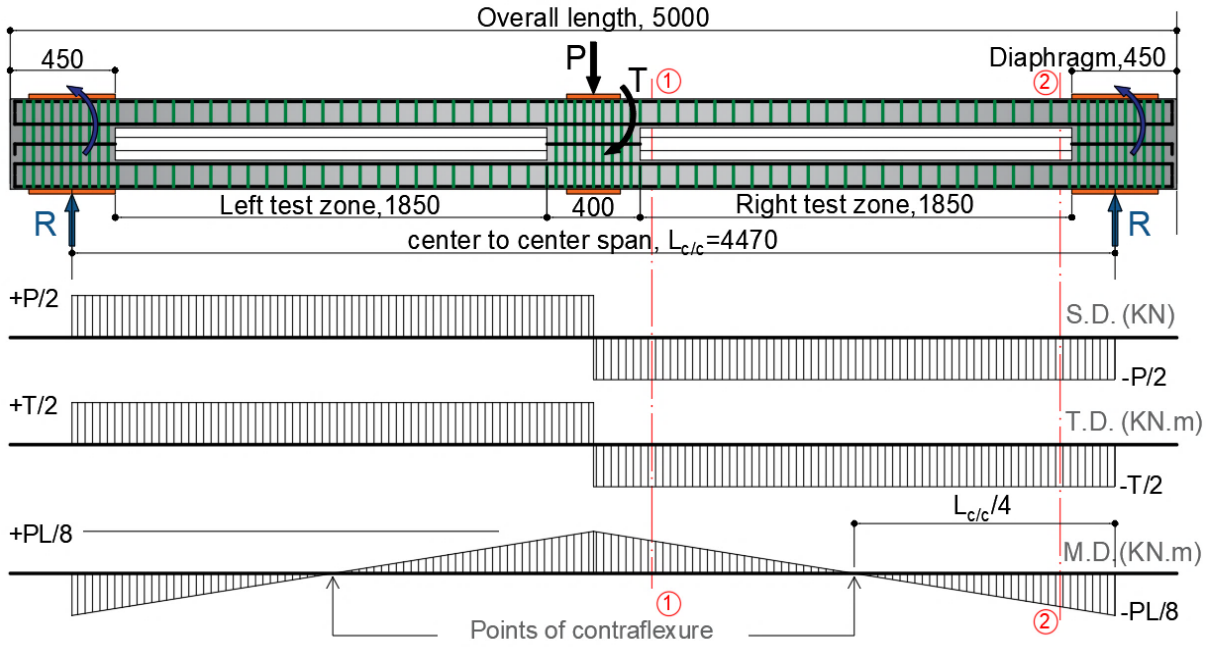

Fig. 3 Shear, torsion, and moment diagrams

2.4. Test Setup and Instrumentation

Figure 4 presents a schematic view of the test setup for a rectangular box-girder under test. All model testing was carried out at the laboratory of the Civil Engineering Department of Salahaddin University. Two new supports were constructed using welded steel frames to newly casted reinforced concrete footings. Further, two steel frames for gripping specimen ends, one steel lever arm, and two auxiliary frames for fixing instrumentations were fabricated and used to ease the conduction of the experiments. In addition, for the connections of the lever arm and support frames, strong bolts were used.

The instrumentations were mainly concentrated in the vicinity of the middle and support sections and at the quarter span to provide detailed results of deflection, twists, and strains. At both middle and support sections, four strain gauges were fixed to the center of the outer legs of the stirrups in addition to another four strain gauges for the four longitudinal corner bars. Besides, eight concrete strain gauges with a gauge length of 80mm were mounted on the concrete surface at 45-degrees to the beam axis, measured in a counterclockwise direction to quantify concrete surface principal strains. Further, six LVDTs were also fastened to the concrete surface at the other part of the test zone, and these are used to record the average crack widths and/or as a supplementary aid to check the concrete strains. The instrumentations for measuring load, concrete surface strain, reinforcement strain, and surface displacements of each specimen were connected to a 48-channel data logger, which works alongside a personal computer and the final recorded data was in the form of CSV file formats.

2.5. Test Procedure

Generally, the following procedure is followed in conducting all the experiments:

I. Before testing any specimen, the midspan and support frames are attached. The midspan frame provides a lever arm of 1.67 m. It transfers the eccentric load from the application center-point of the machine actuator with a capacity of 2500 kN to the center of the specimens.

II. After checking the tolerances and fixing each specimen, the remaining instrumentations, including the concrete strain gauges and the KPM-LVDTs, are fastened to their locations.

III. An auxiliary frame independent of the rest of the test frame is used for the right test zone to provide a stable base for the operation of KTR-LVDTs. Displacement measurements are taken using a total of 16 LVDTs and considering two LVDTs for each face of the beam at each section.

IV. Due to symmetry, the highlighted test zone on the left side of the specimen is utilized for the measurements related to cracks, crack propagations, number, and width of cracks.

V. The load is applied at a rate of 5 kN/min, and a compression load cell of 50-ton capacity is used to record the applied vertical loads.

VI. The data from the LVDTs, load cell, and strain gauges which produce deflection, angle of twist, concrete, and reinforcement strains, is automatically measured and recorded by the automatic 48-channel data logger. The raw data is then processed, and required relations are extracted out.

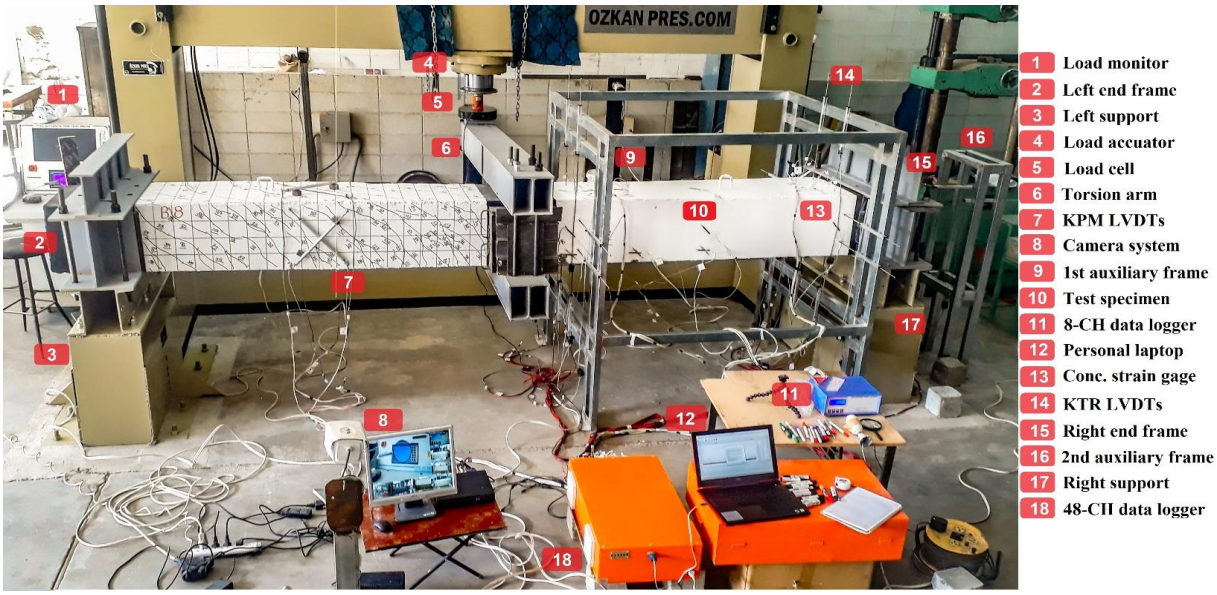

Fig. 4 Schematic view of the test setup

Table 5 Principal test results

Specimens	P_{cr}, kN	Δ_{cr}, mm	P_u, kN	Δ_u, mm	T_{cr}, kN.m	φ_{cr}, rad	T_u, kN.m	φ_u, rad
B-20	48	0.83	176	45.03	80.16	0.001	293.92	0.096
B-23	60	6.85	149	35.77	100.20	0.001	248.83	0.058
B-24	47	0.37	79	6.33	78.49	0.001	131.93	0.033
B-25	30	0.816	104	24.995	50.10	0.001	174	0.061

3. Results and Discussion

Table 5 presents the principal test results, which includes the cracking load (P_{cr}), deflection at cracking (Δ_{cr}), ultimate load (kN), maximum deflection (Δ_u), cracking torque ($kN.m$), twist at cracking (φ_{cr}), ultimate torque ($kN.m$), and maximum twist (φ_u).

3.1. Load-Deflection Behavior

Figure 5 shows the load-deflection responses for all the samples. The circular (o), triangular (Δ), square ($\square$), and the ($\times$) signs represent the cracking load, yield of longitudinal bars, the yield of steel stirrups, and ultimate strain of concrete at 3000 micro-strains, respectively.

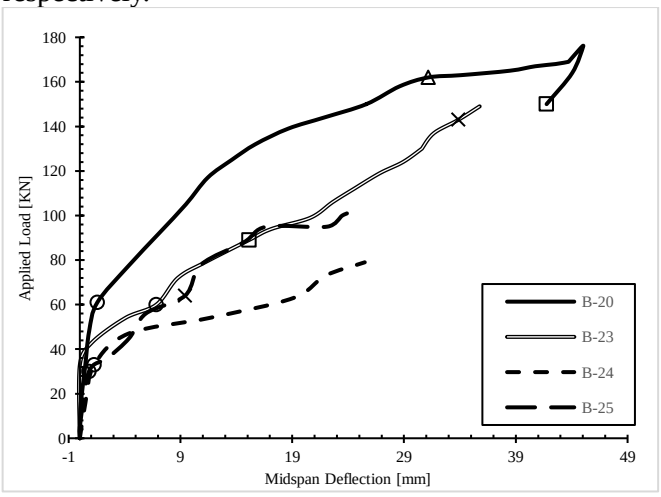

Fig. 5. Load-deflection relationships

Generally, the relationship is steep and linear before and after cracking (denoted by circular marks), except in B-20, entirely steel-reinforced. Hence, a curvilinear trend represents the stage after cracking. The linear trends could be attributed to the linear tensile response of HSC concrete and because the flexural behavior is mainly controlled by the response of longitudinal BFRP-reinforcement in each specimen. However, the post-cracking nonlinear trend in B-20 refers to the more ductile and nonlinear behavior of steel reinforcements used. The ultimate flexural capacities range from 79 to 176 kN, and the ultimate deflections were between 6 to 45 mm. In B-23, there is a shift in the position of the circular mark, indicating that the first crack could have occurred due to torsion but not flexure and that the first crack occurred farther from midspan due to a combination of torsional shear and bending stresses. After the flexural cracking initiates, flexural stiffness drops significantly.

B-20 (with steel reinforcement) shows 15% higher flexural capacity than B-23 (with BFRP bars and steel stirrups), 176 kN vs. 149 kN, respectively. However, surprisingly, the final deflection was higher in the former than the latter, 45.04mm compared to 35.77mm. However, a closer look at the curves reveals that at an equivalent loading of, say 149kN, the total deflection in B-20 was only 25mm compared to 35mm in B-23. Hence, it can be stated that the deflection of a BFRP-reinforced beam is larger for equivalent loadings in comparison to a steel-reinforced counterpart as expected theoretically.

B-24, with hollow cores throughout (i.e., without the diaphragms), offers the least ultimate flexural

capacity of 79 kN, representing only about half of the total capacity of B-23. This proves that B-24 fails prematurely due to a kind of support bearing failure as a result of excluding the diaphragms, which will be further discussed in Section 2.5. The first crack in B-24 also occurred earlier than that of B-23, 47 kN vs. 60 kN, indicating again the effect of excluding the diaphragms, which weakens the resistance of the specimen in bearing the applied loads, and hence the first crack appeared earlier, even at relatively very smaller deflections. As B-24 bears the least ultimate load, therefore, its final deflection was also the least, 6.33mm, compared to all the other specimens.

To assess the effect of filling the hollow cores, B-25, in which no void filler is used, is compared to B-23, utilized with a low-density Styrofoam. The ultimate flexural capacity of B-25 was 104 kN, which constitutes about 70% of the ultimate capacity of B-23. Similarly, the flexural cracking strength of B-25 scores less than that of B-23, 30 kN compared to 60 kN, which is lower by 50%. This result indicates that even Styrofoam has a negligible density. However, when used as a void-filler, it has a substantial role as a confinement medium to enhance the flexural resistance of the surrounding reinforced concrete webs and flanges.

3.2. Torque-Twist Response

The torque-twist curves are extracted from the data of the same LVDTs used for the load-deflection curves, as represented by Figure 6. The symbols represent the same designations as those used for the load-deflection curves.

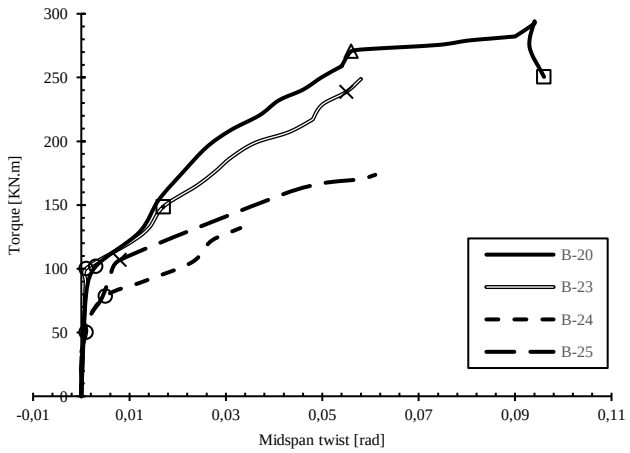

Fig. 6. Torque-twist relationships

As it can be seen, the torque-twist relationships come in the same order as those for the flexural responses, with B-20 and B-24 occupying the upper and lower bounds, respectively. There was a wide scatter in the ultimate torsional capacities, ranging from 132 to 294 kN.m and the ultimate twists were between 0.033 to 0.096 radians.

B-20, which acts as a control specimen in this study, shows higher torsional capacity than B-23, 249 kN.m vs. 194 kN.m, which accounts for a difference of 22%, and the twist angles were also larger in the former than the latter, 0.096 compared to 0.058 radians, respectively. This indicates that replacing steel longitudinal bars with lower-modulus BFRP bars will result in a drop in the total torsional capacity by almost 22%. Conservatively, it could be stated that the drop in the total torsional capacity of BFRP-longitudinally reinforced box-girders compared to steel-reinforced counterparts is analogous to the drop in the elastic modulus of BFRP bars as opposed to steel bars.

As expected, the specimen with diaphragms, B-23, performs stronger than the specimen without diaphragms, B-24. B-23 bears a total torque of 249 kN.m while B-24 resists torques up to 132 kN.m, nearly about half that of B-23. As B-24 fails prematurely due to excluding the diaphragms, the final twists were higher in B-23 due to its bearing for more torques than B-24, respectively (0.058 vs. 0.033). The much lower torsional performance of B-24 in comparison with B-23 proves the practical significance of providing the midspan and end diaphragms in box-girders in resisting the applied torsional and combined loadings.

Comparing the specimen with Styrofoam, B-23, to that without Styrofoam, B-25, it can be seen that the torsional capacity dropped from 249 kN.m to 174 kN.m; however, the ultimate twist remains about the same, with a slightly higher value for B-25 compared to B-23, 0.061 vs. 0.058 radians. It can be deduced that if a box-girder is not provided with a void-filler, then the ultimate torsional capacity will drop by about 30%. In other words, a void-filler such as Styrofoam has the potential to enhance the torsional capacity of a box-girder essentially. As in reality, the true-scale box-girders are not provided with any kind of void-fillers, hence for a void-free box-girder, a 30% decrease in the torsional strength should be accounted for when Styrofoam is used as void-filler.

3.3. Torsional Stiffness

Table 6 compares uncracked (K_{un}) and cracked (K_{cr}) torsional stiffness for the tested specimens. It can be stated that a member which achieves higher torsional strength than another may not necessarily achieve the same priority in terms of stiffness. For instance, the results reveal that B-23 with BFRP bars and steel stirrups scores the highest pre-cracking torsional stiffness of 100,200 kN.m^2, followed by 80,160 kN.m^2 in B-20 with entirely steel reinforcement. As the pre-cracking torsional strength and stiffness in B-23, which is higher by 25% than that of B-20, could not be easily interpreted theoretically; therefore, further experimental studies are recommended to be conducted. On the other hand, B-23 is stiffer than B-20 by about 24% regarding the post-cracking torsional

stiffnesses. However, this enhanced post-cracking stiffness could be easily attributed to the lower angle of twist of B-23 compared to that of B-20. However, the post-cracking stiffness trend might change when the torsional stiffness at 85% of ultimate torque is considered, as is the case in B-23 and B-20. The computations in the last column of Table 6 demonstrate that at 85% of comparable loadings, the torsional stiffness of B-20 is higher by (100-73=27%). This indicates that at comparable loadings in the post-cracking stage before failure, steel-reinforced box-girders are reasonably stiffer by 27% than their BFRP-longitudinally reinforced specimens.

Table 6 Comparison of torsional stiffnesses

B.	T_{cr}, kN.m	φ_{cr}, rad	T_u, kN.m	$T_{u,0.85}$, kN.m	φ_u, rad	$\varphi_{u,0.85}$, rad	K_{un} kN.m^2	K_{cr} kN.m^2	$K_{cr,0.85}$ kN.m^2	$\frac{K_{un}}{K_{un(B-20)}}$	$\frac{K_{cr}}{K_{cr(B-20)}}$	$\frac{K_{cr,0.85}}{K_{cr(B-20)}}$
20	80.16	0.001	293.92	250.5	0.094	0.050	80,160	2,298	3,476	1.00	1.00	1.00
23	100.2	0.001	248.83	211.5	0.058	0.045	100,200	2,608	2,530	1.25	1.24	0.73
24	78.49	0.001	131.93	112.0	0.033	0.025	78,490	1,670	1,417	0.98	0.73	0.41
25	50.10	0.001	174.00	147.9	0.061	0.040	50,100	2,065	2,508	0.63	0.90	0.72

where K_{un} = uncracked torsional stiffness = T_{cr}/ϕ_{cr} and K_{cr} = cracked torsional stiffness = $(T_u - T_{cr})/(\varphi_u - \varphi_{cr})$

The least torsional stiffness after cracking is attributed to B-24. This means that the exclusion of diaphragms has a substantial effect on the post-cracking torsional stiffness, and hence this option should be considered with great care in reality. Last and not least, the post-cracking torsional stiffness of B-25 with a decline of only 10% shows that it is not substantially affected compared to that of B-20.

3.4. Crack Pattern

3.4.1. First Crack

Before testing, the beams were painted white so that the crack development could be easily observed. Each specimen includes two test zones located on each side of the midspan diaphragm. One of these zones was highlighted to form a grid of equally spaced cells in both longitudinal and transverse directions on three faces only (front, top, and rear). The other test zone was not highlighted as similar cracks were expected to form due to symmetry on either side

Generally, the first cracks appeared at the bottom face and then extended towards the tensile flexural zone of the vertical faces and then inclined at approximately 45-degrees to the axis of the members. Table 7 presents the details of the first cracks in the tested specimens. The first cracks in B-23 and B-20, which have the highest flexural and torsional stiffnesses, were a combination of torsional shear and flexural-shear cracks and occurred at 60 and 48 kN in the range of middle to quarter span, respectively. These cracks were formed in both the flexural tensile zone and the shear webs concurrently and thus denoted by "torsional-shear" and "flexural-shear" cracks. While the "flexural shear" cracks initiated vertically in the webs and later inclined; however, the "torsional shear" cracks in B-20 were diagonal cracks.

Table 7 Details of first cracks

Beams	P_{cr}, kN	Type	Nearest position
B-20	48	Torsional shear	Mid-Quarter span
B-23	60	Flexural-shear	Mid-Quarter span
B-24	47	Flexure	Mid-Quarter span
B-25	30	Flexure	Midspan

The first cracks in B-24 and B-25 were initiated earlier than the first cracks in B-23 and B-20. In B-24, the first crack appears at 47 kN vertically near quarter-span, and the earliest crack occurs vertically in the webs in B-25 at the lowest loading of 30 kN only, and hence these cracks are named *flexural* cracks. These cracks reflect the direct effect of bending due to the lower elastic modulus of the BFRP reinforcements, in addition to the exclusion of diaphragms in B-24 and the void fillers in B-25. Additionally, the initial flexural crack in B-25, which occurs close to the midspan, could be attributed to the effect of using lower modulus BFRP bars and the exemption of the void-fillers, which combinedly lead to evident midspan deflections.

3.4.2. Crack Propagation

The crack marks are re-drawn by a CAD tool to better visualize the crack pattern on all faces, understand the crack pattern, and easily measure the angle between the cracks and the axis of the beam (see Figure 7). The main trends show that the vast majority of the cracks were due to torsion, which dominates the other combined actions. In specimens B-23, B-24, and B-25, the occurrence of the flexural cracks in the webs and the bottom face could be partly attributed to the use of BFRP longitudinal bars, which have a lower modulus of elasticity compared to steel and are thus prone to more relative deflections. There were more intensive cracks on the two vertically loaded web (LW) and the unloaded web (UW) sides, denoted by back and front faces in Figure 7, respectively" rather than the horizontal top and bottom faces. More cracks form on the LW face rather than the UW face since diagonal tension stresses due to transverse shear and torsion were additive on the LW side but subtractive on the UW one. With more progress in loading, the initial cracks were extended to the upper portions of the webs and then jumped to the top face, and eventually, the cracks on all faces were reached each other forming complete spirals in a helical form.

B-20 presents the most densified and regular arrows of diagonal cracks and complete-formed spirals

showing its improved torsional capacity compared to other specimens. This box-girder could withstand the highest loading and eventually witnessed excessive spalling and crushing of concrete compression diagonals close to the midspan, as indicated by the hatched area in Figure 7. On the contrary, B-24 shows the most widespread and irregular cracks, incomplete spiral cracks, and no signs of spalling or crushing, reflecting its lowest torsional capacity amongst the other specimens. A widened spiral crack extended from the quarter span to the diaphragm-removed ends causing the premature failure of this specimen. The crack pattern of B-23 was uniform and regular, but there were relatively much fewer cracks in B-23 as opposed to B-20. The above shows that the extent of cracks is a good indication of the strength; the more the cracks, the stronger the member and vice versa.

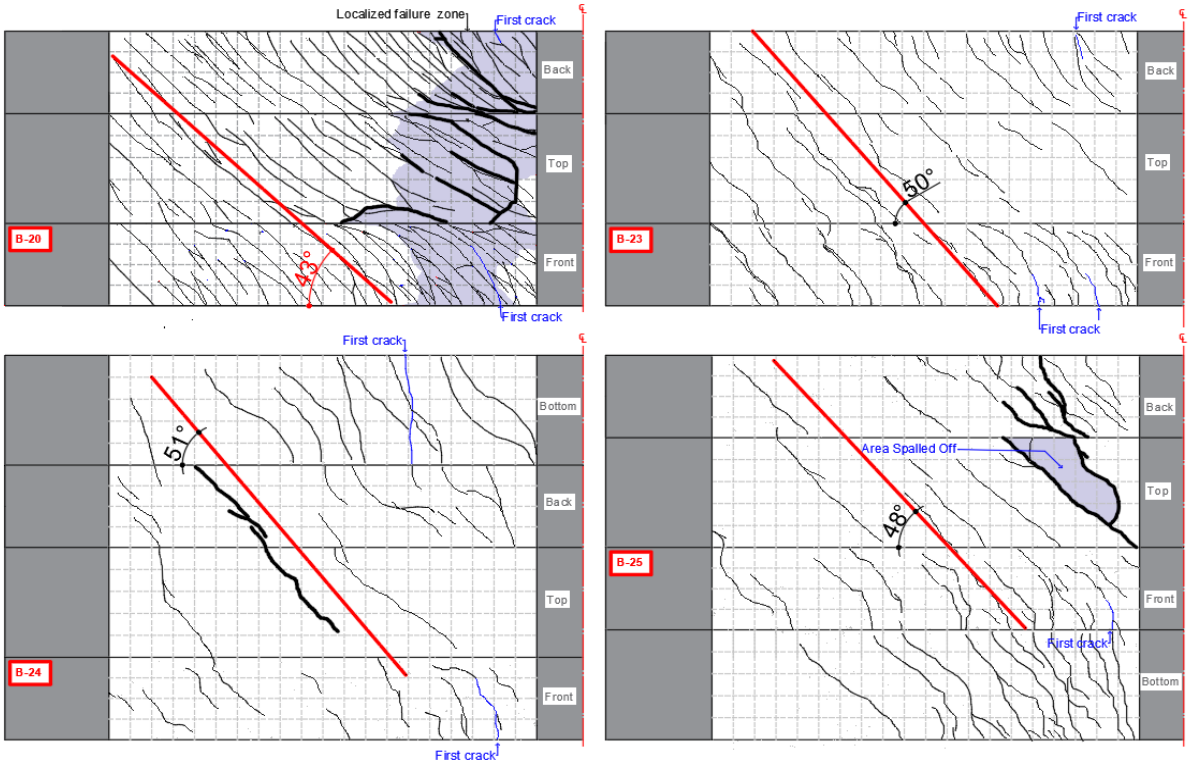

Fig. 7 Schematics of crack pattern and average strut angles

3.4.3. Crack Inclination Angle

In all the specimens, the reinforcement was approximately equally distributed both longitudinally and transversally with the intention that when cracks formed, the angle of diagonal concrete struts remains approximately around 45 degrees. The torsional cracks on all the faces had approximate inclinations of 43, 50, 51, and 48 degrees for the specimens B-20, B-23, B-24, and B-25, respectively, measured clockwise from the beam axis for the left-hand test zone as is shown previously in Figure 7. The crack inclination angle for the steel-reinforced specimen does not deviate much from the recommended 45-degrees angle specified by the ACI 318 Code [26]. The average crack inclination angle for other BFRP-longitudinally reinforced specimens, which is about 50 degrees, also varies within the ACI range of 30-degrees to 60-degrees. However, as the average value is higher than 45-degrees, this indicates that the performance of the BFRP-reinforced box-girders is lower than that of the steel-reinforced counterpart. On the other hand, as there are minor deviations in the crack angles among the three BFRP-reinforced specimens, hence it can also be concluded that the cracking angle of the BFRP-reinforced specimens is only slightly affected by the method of void-filling or the exemption or the consideration of the diaphragms.

3.5. Analysis of Failure Modes

In general, all the specimens experienced yielding of concrete and steel stirrups before failure; however, the rate of damage was severe in the fully steel-reinforced specimen than the other BFRP-longitudinally reinforced specimens. As depicted by Figure 8 (left), in B-20, the failure zone concentrated near the midspan, which shows a combination of wide cracks, severe crushing and spalling of concrete cover accompanied by yielding of longitudinal steel bars transverse steel stirrups. B-23, as shown in Figure 8 (right), presents fewer cracks and few spalling prior to failure compared to B-20; its failure mode is distinguished mainly by crushing concrete compression struts in the loaded web side close to the midspan diaphragm.

Regarding B-24, the failure occurs close to the supports, as shown in Figure 9 (left), due to high concentrated stresses at the diaphragm-less ends that

lead to premature bearing failure at the supports. Eventually, this specimen was unable to attain its full potential capacity. The failure mode in the specimen without the void-filling substance, B-25, concentrated close to the midspan due to widened cracks at the top and loaded web side and spalling at the top face as shown by Figures 7 and 9 (right).

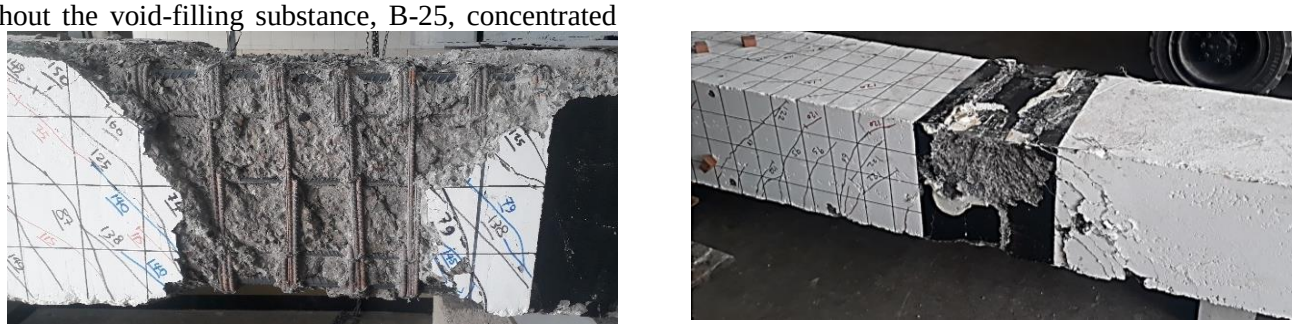

Fig. 8 Failure zones in B-20 (left) and B-23 (right)

Fig. 9 Failure zones in B-24 (left) and B-25 (right)

4. Conclusions

The vast majority of torsional studies, to date, mainly deal with solid concrete members reinforced with conventional steel reinforcement under either pure torsion, torsion with shear, or torsion combined with bending action only. Further, due to the complexity of the problem, only a few studies have addressed solid or hollow members under combined loadings using conventional steel reinforcement. FRP-related works also focus mostly on tests of FRP-reinforced members under pure torsion. Consequently, FRP codes of practice and design guidelines, while including provisions for the case of pure torsion, but all lack provisions regarding the torsional strength of box-girders under the more practical actions of torsion, shear, and bending altogether. This is partly because FRP is a new-age material but mainly because tests of specimens under combined loadings are complex, costly, and time-worthy. With this milestone, the current research attempts to put the first steps forth towards exploring this essential domain. Experimental tests on three HSC box-girders reinforced with BFRP bars, steel stirrups, and one traditionally steel-reinforced companion were conducted under torsion, shear, and bending. The variables were the type of longitudinal reinforcement (BFRP vs. mild steel), the role of middle and support-diaphragms, and the effect of filling the internal cores with Styrofoam compared to the void-free case. The main conclusions are:

1) The entirely steel-reinforced specimen, B-20, offers a higher flexural and torsional performance by 18% than its BFRP-longitudinally reinforced counterpart, B-23. The exclusion of diaphragms as in B-24 leads to the lowest flexural and torsional capacity of 79 kN and 132 kN.m, respectively, which constitutes a decrease of 53% in the total capacities. In addition, leaving the internal space unfilled as in B-25 adversely affects the flexural and torsional strengths leading to a drop of 30% in the ultimate capacities.

2) Although the lower elastic modulus of the BFRP-longitudinally reinforced specimen, surprisingly, the ultimate deflection in B-23 was less than that of B-20, 36mm vs. 45mm. This was due to the resistance of B-20 to more loadings than B-23. However, the deflection values at comparable loadings showed a reverse trend, 25 mm in B-20 compared to 36 mm in B-23, i.e., at comparable loadings, the deflection of the steel-reinforced specimen is lower than its BFRP longitudinally-reinforced pair as expected. The same findings for the deflections also apply to the angles of twist and the torsional stiffness values.

3) First cracking in the weakened specimens (due to either the removal of the diaphragms or the void-fillers) occurred at earlier loadings due to flexure only at 30 kN and 47 kN in B-25 and B-24, respectively. In the other specimens, B-23 and B-20 (both with void-fillers and diaphragms), the first cracks appear at higher loadings of 48 kN and 60 kN, respectively. The latter two specimens also bear higher ultimate loadings than the former two.

4) The inclined torsional crack angles were in the range of 43 to 51 degrees. The crack angle in the

BFRP-longitudinally reinforced box-girders (B-23, B-24, and B-25) were about 50-degrees, while in the steel-reinforced one, B-20, it was about 43-degrees. This indicates that the lower the crack inclination is, the more enhanced the performance of the box-girders could be.

5) This work was limited to rectangular non-prestressed HSC box-girders without overhangs subjected to torsion, shear, and bending. Therefore, further research is needed to study the behavior of trapezoidal prestressed HSC box-girders with or without overhangs reinforced entirely with FRP bars and FRP stirrups under the combined loading. Moreover, from the authors' perspective, it is essential that further experiments need to be conducted in this emerging field in the future to supplement the FRP codes and design guidelines with a broader database.

Acknowledgment

The authors acknowledge the cooperation and support provided by the Concrete and Structures Lab of Salahaddin University and the Mechanics of Materials Lab of Koya University.

Notation

$f_c^{'}$ - Compressive strength of concrete cylinders, MPa

f_{fu},ε_{fu}- ultimate tensile strength and strains of FRP bars;

f_y,ε_y - yield strength and strains of steel bars;

f_u,ε_u - ultimate tensile strength and strains of steel bars;

A_l, A_t - Longitudinal and transverse reinf., mm^2;

ρ_l, ρ_t - Longitudinal and transverse reinforcement ratio;

A_{oh} - Area enclosed by the outer legs of stirrups, mm^2;

p_h - Periphery enclosed by outer stirrup legs, mm;

s - center to center distance of vertical stirrups, mm;

T_{cr} - measured cracking torque of beam specimens;

φ_{cr} - measured angle of twist at cracking;

$T_{cr,0.85}$ - Cracked torque at 85 percent of ultimate torque;

$\varphi_{cr,0.85}$ - Angle of twist at 85 percent of ultimate torque;

T_u - measured ultimate torque of beam specimens;

φ_u - measured angle of twist at ultimate torque

References

[1] ACI440.1R-15. Guide for the Design and Construction of Structural Concrete Reinforced with Fiber-Reinforced Polymer Bars. American Concrete Institute, ACI Committee 440. [S]. Farmington Hills, USA, 2015.

[2] ABBOOD IS, ODAA SA, HASAN KF, and JASIM MA. Properties evaluation of fiber reinforced polymers and their constituent materials used in structures – A review. [J] *Materials Today: Proceedings*, 2021, 43: 1003-1008. https://doi.org/10.1016/j.matpr.2020.07.636

[3] NANNI A. Flexural behavior and design of RC members using FRP reinforcement. [J] *Journal of Structural Engineering*, ASCE, 1993, 119(11): 3344-3359. https://doi.org/10.1061/(ASCE)0733-9445(1993)119:11(3344)

[4] CAN/CSA(S-806). Design and construction of building structures with fiber-reinforced polymers. [S] CSA Group, Canada, 2nd edition, 2017.

[5] NCHRP. *NCHRP Report 620: Development of Design Specifications and Commentary for Horizontally Curved Concrete Box-Girder Bridges* [M]. National Cooperative Highway Research, Transportation Research Board, Washington, 2008: 21.

[6] AMULU CP, and EZEAGU CA. Combined Torsion, Bending and Shear Analysis in Reinforced Concrete. [J] *International Journal of Advanced Trends in Technology, Management, and Applied Science*, 2016, 2(6): 45-65.

[7] DEIFALLA AF, AWAD A, et al. Effectiveness of externally bonded CFRP strips for strengthening flanged beams under torsion: An experimental study.[J] *Engineering Structures*, 2013, 56: 2065-2075. https://doi.org/10.1016/j.engstruct.2013.08.027

[8] RAGAB KS, and EISA AS. Torsion Behavior of Steel Fibered High Strength Self Compacting Concrete Beams Reinforced by GFRB Bars. [J] *International Journal of Civil, Environmental, Structural, Construction and Architectural Engineering*, 2013, 7(9): 659-669. https://doi.org/10.5281/zenodo.1087620

[9] EL-AWADY E, HUSAIN M, and MANDUOR S. FRP-Reinforced Concrete Beams Under Combined Torsion and Flexure. [J] International *Journal of Engineering Science and Innovative Technology*, 2013, 2(1): 384-393

[10] SALEH A, HAMED M, et al. The effect of replacing steel reinforcements with GFRP on the torsional behavior of RC L-beams. [C] *Second Conference on Smart Monitoring, Assessment and Rehabilitation of Civil Structures*, 2013.

[11] DEIFALLA AF, HAMED M, et al. Exploring GFRP bars as reinforcement for rectangular and L-shaped beams subjected to significant torsion: An experimental study. [J] *Engineering Structures*, 2014, 59: 776-786. https://doi.org/10.1016/j.engstruct.2013.11.027

[12] MOHAMED HM, CHAALLAL O, and BENMOKRANE B. Torsional moment capacity and failure mode mechanisms of concrete beams reinforced with carbon FRP bars and stirrups. [J] *Journal of Composites for Construction*, 2015, 19(2)ж 515. https://doi.org/10.1061/(ASCE)CC.1943-5614.0000515

[13] MOHAMED HM, and BENMOKRANE B. Torsion behavior of concrete beams reinforced with GFRP bars and stirrups. [J] *Structural Journal*, 2015, 112(5): 543-552.

[14] ZHOU J, SHEN W, and WANG S. Experimental Study on Torsional Behavior of FRC and ECC Beams Reinforced with GFRP Bars. [J] *Construction and Building Materials*, 2017, 152: 74-81. https://doi.org/10.1016/j.conbuildmat.2017.06.131

[15] HADHOOD A, GOUDA MG, et al. Torsion in concrete beams reinforced with GFRP spirals. [J] *Engineering Structures*, 2020, 206: 110174. https://doi.org/10.1016/j.engstruct.2020.110174

[16] ASTM C31/C31M, Standard Practice for Making and Curing Concrete Test Specimens in the Field. ASTM International, West Conshohocken, PA, USA, 2019.
[17] FIB Model Code-2010, FIB Model Code for Concrete Structures, Fédération Internationale du Béton, 2013.
[18] ASTM C39/C39M, Standard Test Method for Compressive Strength of Cylindrical Concrete Specimens. American Society for Testing and Materials, Pennsylvania, PA, 2018.
[19] ACI 363R-10. Report on High-Strength Concrete, American Concrete Institute (ACI). [S] Detroit, MI, USA, 2010.
[20] ASTM C469-17. Standard Test Method for Splitting Tensile Strength of Cylindrical Concrete Specimens. ASTM International. [S] West Conshohocken, PA, USA, 2017.
[21] ASTM C496/C496M. Standard Test Method for Splitting Tensile Strength of Cylindrical Concrete Specimens. ASTM International. [S] West Conshohocken, PA, USA, 2017.
[22] ASTM C78/C78M. Standard Test Method for Flexural Strength of Concrete (Using Simple Beam with Third-Point Loading). ASTM International. [S] West Conshohocken, PA, USA, 2018.
[23] GB/T. 228-2002: Chinese Standard translated into English. (GBT 228-2002, GB/T228-2002, GBT228-2002): Metallic materials - Tensile testing at ambient temperature. [S] China, 2014. https://www.chinesestandard.net.
[24] ASTM A-370. Standard Test Methods and Definitions for Mechanical Testing of Steel Products. ASTM International. [S] West Conshohocken, PA, USA, 2017.
[25] Eurocode 2. Design of Concrete Structures, part 1: General Rules and Rules for Buildings. [S] Thomas Telford, London, 1992.
[26] ACI 318-19M, ACI 318-19M: Building Code Requirements for Structural Concrete and Commentary. [S] Farmington Hills: ACI Committee 318, 2019.

参考文:

[1] 国际交流协会 440.1 电阻-15。用纤维增强聚合物钢筋增强的结构混凝土的设计和施工指南。美国混凝土学会，国际交流协会委员会 440。[S]。美国法明顿山，2015.
[2] ABBOOD IS、ODAA SA、HASAN KF 和 JASIM MA。纤维增强聚合物及其结构中使用的组成材料的性能评估——综述。[J] 今日材料：论文集，2021，43：1003-1008。 https://doi.org/10.1016/j.matpr.2020.07.636
[3] NANNI A. 使用玻璃钢加固的 RC 构件的弯曲行为和设计。[J] 结构工程学报, ASCE, 1993, 119(11): 3344-3359. https://doi.org/10.1061/(ASCE)0733-9445(1993)119:11(3344)
[4] 能够/CSA(秒-806)。用纤维增强聚合物设计和建造建筑结构。[S] CSA 集团，加拿大，第 2 版，2017.
[5] NCHRP。NCHRP 报告 620：水平弯曲混凝土箱梁桥设计规范的制定和评论 [M]。国家合作公路研究，交通研究委员会，华盛顿，2008：21。
[6] AMULU CP 和 EZEAGU CA。钢筋混凝土中的组合扭转、弯曲和剪切分析。[J] 国际技术、管理与应用科学前沿趋势杂志, 2016, 2(6): 45-65.
[7] DEIFALLA AF、AWAD A 等。外粘碳纤维布加固翼缘梁受扭效果的试验研究[J] 工程结构, 2013, 56: 2065-2075. https://doi.org/10.1016/j.engstruct.2013.08.027
[8] RAGAB KS 和 EISA AS。GFRB 钢筋加固的钢纤维高强度自密实混凝土梁的扭转行为。[J] 国际土木、环境、结构、建筑与建筑工程杂志，2013, 7(9): 659-669. https://doi.org/10.5281/zenodo.1087620
[9] EL-AWADY E、HUSAIN M 和 MANDUOR S. 玻璃钢钢筋混凝土梁在组合扭转和弯曲下。[J] 国际工程科学与创新技术学报, 2013, 2(1): 384-393
[10] SALEH A, HAMED M, 等。用玻璃钢代替钢筋对 RC 升梁扭转性能的影响。[C] 第二届土木结构智能监测、评估和修复会议，2013。
[11] DEIFALLA AF, HAMED M, 等。探索玻璃钢钢筋作为承受显着扭转的矩形和 L 形梁的钢筋：一项实验研究。 [J] 工程结构, 2014, 59: 776-786. https://doi.org/10.1016/j.engstruct.2013.11.027
[12] MOHAMED HM、CHAALLAL O 和 BENMOKRANE B. 用碳玻璃钢钢筋和箍筋加固的混凝土梁的扭矩容量和破坏模式机制。[J] 建筑复合材料学报, 2015, 19(2): 515. https://doi.org/10.1061/(ASCE)CC.1943-5614.0000515
[13] MOHAMED HM 和 BENMOKRANE B. 用玻璃钢钢筋和箍筋加固的混凝土梁的扭转行为。[J] 结构学报, 2015, 112(5): 543-552.
[14] 周杰、沉伟和王顺. 玻璃钢钢筋加固 FRC 和 ECC 梁扭转行为的试验研究。[J] 建筑建材, 2017, 152: 74-81. https://doi.org/10.1016/j.conbuildmat.2017.06.131
[15] HADHOOD A, GOUDA MG, 等。用玻璃钢螺旋加固的混凝土梁的扭转。[J] 工程结构, 2020, 206: 110174. https://doi.org/10.1016/j.engstruct.2020.110174
[16] ASTM C31/C31 米，现场制作和固化混凝土试样的标准做法。ASTM 国际，西康绍霍肯，宾夕法尼亚州，美国，2019.
[17] 金融情报局模型代码-2010，混凝土结构金融情报局模型代码，国际混凝土联合会，2013.
[18] ASTM C39/C39 米，圆柱形混凝土试样抗压强度的标准测试方法。美国测试与材料协会，宾夕法尼亚州，宾夕法尼亚州，2018.
[19] 国际交流协会 363 电阻-10。高强度混凝土报告，美国混凝土协会 (国际交流协会)。[S] 美国密歇根州底特律，2010.
[20] ASTM C469-17。圆柱形混凝土试样劈裂抗拉强度的标准试验方法。ASTM 国际。[S] 美国宾夕法尼亚州西康绍霍肯，2017.
[21] ASTM C496/C496 米。圆柱形混凝土试样劈裂抗拉强度的标准试验方法。ASTM 国际。[S] 美国宾夕法尼亚州西康绍霍肯，2017.
[22] ASTM C78/C78 米。混凝土弯曲强度的标准试验方法（使用具有第三点载荷的简单梁）。ASTM 国际。[S] 美国宾夕法尼亚州西康绍霍肯，2018.
[23] 国标/吨. 228-2002：中文标准译成英文。（GBT 228-2002、国标/吨 228-2002、GBT228-2002）：金属材料 - 环境温度下的拉伸试验。[S] 中国，2014。https://www.chinesestandard.net。
[24] ASTM 一种-370。钢产品机械试验的标准试验方法和定义。ASTM 国际。 [S] 美国宾夕法尼亚州西康绍霍肯，2017.
[25] 欧洲规范 2. 混凝土结构设计，第 1 部分：一般规则

和建筑物规则。[S] 托马斯·特尔福德，伦敦，1992.
[26] 国际交流协会 318-19M、国际交流协会 318-19 米：结构混凝土的建筑规范要求和注释。[S] 法明顿山：国际交流协会委员会 318，2019.